sustainability

Article

Optimizing Water-Light Complementary Systems for the Complex Terrain of the Southwestern China Plateau Region: A Two-Layer Model Approach

Zhikai Hu [1], Zhumei Luo [1,*], Na Luo [2], Xiaoxv Zhang [1], Haocheng Chao [1] and Linsheng Dai [1]

[1] Department of Metallurgy and Energy Engineering, Kunming University of Science and Technology, Kunming 650500, China; huzhikaihuzhiqiang@outlook.com (Z.H.); dynzhang@163.com (X.Z.); 20212202208@stu.kust.edu.cn (H.C.); dailinsheng163@163.com (L.D.)
[2] School of Earth Science and Engineering, Hohai University, Nanjing 210024, China; ruora2003@163.com
* Correspondence: luozhumei@163.com

Abstract: This study aimed to optimize the real-time, short-term dispatch of water-light complementary systems in plateau areas. A two-layer nested improved particle swarm optimization-stepwise optimization algorithm trial (IPSO-SOAT) model was devised to address the challenges posed by the intermittent, volatile, and random characteristics of renewable energy, leading to difficulties in renewable energy consumption and severe power cuts. The model, was employed to optimize the load distribution of complementary system power stations. The outer layer of the model employs an improved particle swarm optimization algorithm to introduce uncertainty and enhance prediction accuracy. Additionally, regional optimization and robust optimization were incorporated to improve prediction reliability. The objective function was aimed at minimizing the residual load variance. The inner layer of the model employs a stepwise optimization algorithm, coupled with a two-dimensional coding strategy for the hydropower unit, to optimize the operating status of the hydropower station unit. The objective function in this layer minimizes flow consumption. A water-light complementary system was comprehensively analyzed in the context of the southwestern plateau region, considering the complex terrain characteristics. By comparing three scenarios, the superiority and flexibility of the two-level nested model were visualized. The proposed double-layer nesting model minimizes energy and natural resource consumption while ensuring sustainability, resulting in a reduction of 15,644.265 tons of carbon dioxide emissions per year. This technological innovation makes a significant contribution to sustainable development.

Keywords: two-layer nested optimization algorithm; multi-energy complementarity; clean energy; optimized Ddispatch

check for updates

Citation: Hu, Z.; Luo, Z.; Luo, N.; Zhang, X.; Chao, H.; Dai, L. Optimizing Water-Light Complementary Systems for the Complex Terrain of the Southwestern China Plateau Region: A Two-Layer Model Approach. *Sustainability* **2024**, *16*, 292. https://doi.org/10.3390/su16010292

Academic Editors: Jian Chen, Wen Zhang, Yongliang Liang and Muhammad Mamdouh Kabsha

Received: 16 November 2023
Revised: 18 December 2023
Accepted: 20 December 2023
Published: 28 December 2023

1. Introduction

Sustainable development, as defined by the World Commission on Environment and Development in "Our Common Future", entails a holistic approach to progress by fulfilling current needs without compromising the potential of future generations to satisfy their requirements. The transition to cleaner, more efficient technologies minimizing energy and natural resource usage, often referred to as "zero-emission" or "hermetic" processes, embodies the concept of sustainable development. Energy is a cornerstone of modern economies and the material foundation for human society, playing a pivotal role in a nation's fundamental competitiveness [1]. As the global economy expands rapidly, the demand for energy and resources has been increasing [2], leading to resource shortages and environmental damage. Therefore, renewable energy sources must be explored to address the energy crisis and ecological deterioration, ensure future energy security, and mitigate global warming effects [3]. Solar and wind power generation, owing to their cost-effectiveness, safety, and minimal secondary pollutants, have become leading forms of new energy generation in recent years [4,5].

However, the technology for integrating wind and solar energy into the power grid is still evolving. Direct grid integration poses challenges to grid scheduling and operation, hindering economically viable grid operations [6]. Consequently, the efficiency of clean energy utilization is compromised, and wind and solar resources face abandonment. To counteract this, integrating and synergizing renewable energy sources, using water turbines for rapid regulation, can slow down the changing fluctuations of wind and solar inputs. This approach establishes a high-quality, reliable, and complementary power-generating system, promoting the integration of new energy sources into the grid [7,8]. Effectively connecting new energy consumption to the grid through a regional multi-energy complementary system proves to be a practical solution [9–12].

Another term for multi-energy complementing systems is hybrid energy systems (HESs) [13]. Scheduling program studies encompass complementary real-time short-term scheduling, complementary medium and long-term scheduling, and complementary system planning and design. Previous studies on HES optimization schemes [14] have integrated numerical techniques with energy planning to maximize power plant profitability. However, these studies often lack consideration for nonlinear constraints, such as unit vibration constraints, which are crucial for ensuring safe unit operation. Utilizing the large system decomposition coordination method (LSSDCM) [15] an integrated energy system coordination and optimization framework has been proposed, considering various energy source ratios and optimizing maximum peaking capacity while addressing long- and short-term complementary characteristics. Despite this, the algorithm frequently converges to a local optimum. A multi-objective two-tier model with cost analysis has been proposed, accounting for the distribution, operation, investment, and upkeep of renewable energy sources [16]. Furthermore, a multi-objective model and solution algorithm aiming to maximize operational revenue, minimize waste energy costs, and reduce output volatility were proposed. However, these studies focus solely on the energy production side without accounting for demand considerations [17].

The primary challenge in HES short-term scheduling lies in effectively managing the uncertainty of wind and solar output projections to create a reliable day-ahead generation plan for the complementary system [16]. Both domestic and international scholars have extensively investigated this issue. The long-term complementary operational performance of a large-scale hydro-PV hybrid power plant was improved using stochastic optimization [17]. A two-layer planning model was proposed for generating day-ahead power generation schedules for water-wind complementing systems, considering the uncertainty of wind power forecasts [18]. Furthermore, a stochastic optimization model was proposed for the day-ahead peaking of water-wind-photovoltaic complementary systems, minimizing the peak-to-valley difference of the residual load and applying it to the day-ahead scheduling of a provincial grid in southern China [19]. The model analyzes the prediction error of wind power and photovoltaic power. An improved intelligent hybrid renewable energy management system was developed to effectively utilize local renewable energy [20]. The system incorporates a dynamic decision-making algorithm in the intelligent system micro-controller to determine the optimal combination of local solar and wind energy. Similarly, one study devised decision-making algorithms and conducted 13 case studies to establish and evaluate the management of hybrid renewable energy systems (HRES) [21].

Given the inherent uncertainty in predictions, scheduling decisions in these studies often entail risks. Therefore, the present study proposes an economic dispatch model that integrates robust optimization and regional optimization to accommodate forecast uncertainty. Furthermore, a two-level nested model is employed to efficiently address the growing computational complexity arising from robust optimization and regional optimization in multi-constraint and high-dimensional conditions.

In general, hydropower plants prioritize power generation in the context of "one reservoir for multiple uses" and "one water for multiple uses", encompassing irrigation, flood control, water supply, environmental protection, and shipping, before acting as a regulator in the local multi-energy complementary system [22]. However, most studies have focused on maximizing the hydropower plant's output as the objective function, prioritizing grid regulation over peaking pressure, risking the operational safety of hydropower units, and hindering dispatch implementation. A robust and stable model and strategy are urgently needed to guide daily dispatch generation in regional multi-energy complementary systems [23], given the crucial role of hydropower units in ensuring the safety of hydropower facilities and the power grid.

The main innovations and contributions of this study include: (1) Utilizing a typical daily scenario derived from a cluster statistical analysis of historical data of water-photovoltaic (WPV) co-optimized systems, estimating the uncertainty of hydropower-PV power output in 1-min increments in WPV systems in the Southwest Plateau region; (2) Transforming the uncertainty of PV generation into the residual hydropower loads supplementing hydro-PV systems based on river runoff; (3) Developing a two-layer nested model with multiple solutions for the HPV portion using the inertia-weighted improved particle swarm optimization algorithm and stepwise optimization algorithm trials; (4) Recognizing the significant impact of daily runoff into small or narrow reservoirs on head, incorporating runoff prediction and regional optimization to relate runoff uncertainty characteristics to the output of the regional complementary system; (5) Introducing the Bellman optimization principle, considering unit vibration constraints, and utilizing a stepwise optimization algorithm for trial runs to select the optimal operation scheme of the complementary system for the current situation.

The structure of the essay is as follows: Section 2 presents the theoretical foundation and details of the research technique, along with information on the fluctuation characteristics of PV power plant production across successive periods and the two-layer nested algorithm. Section 3 presents a case study of a regional complementary system in China. Section 4 displays the comparative computational outcomes of the three scheduling scenarios utilizing the aforementioned model. Section 5 summarizes the thesis research.

2. Research Methodology

2.1. Summarize

This study considers the economic operation challenges of the regional multi-energy complementary system, characterized by the imperative of aligning machinery with power needs. Introducing robust optimization and regional optimization facilitates forecasting the load of photovoltaic (PV) power generation and microgrid during real-time operation. The uncertainty in PV power and microgrid load is translated directly into hydropower scheduling decisions by adjusting the output of hydropower units to accommodate changes in PV output while meeting microgrid demand. This enhances the decision-making capacity of the control center, albeit at the cost of escalating dimensionality and nonlinear constraints in short-term hydropower dispatch, particularly in the presence of uncertainty [24]. Devising practical scheduling algorithms that strike a balance between computational accuracy and efficiency remains a significant challenge in the field of short-term hydropower scheduling [25]. This study introduces an innovative approach by developing coupled inertia weights for the bilayer nested optimization approach and particle swarm optimization (PSO) algorithm. This approach enhances solution efficiency and seeks optimal scheduling that reconciles computational accuracy and efficiency. The technical route is illustrated in Figure 1, while the overall framework is depicted in Figure 2.

The comprehensive framework considers incoming water to hydropower plants, changes in grid load, and variations in PV plant output when designing the hydropower generating plan for regional small hydropower plants. Leveraging historical data from a multi-energy complementary system in the plateau area of Southwest China, the K-nearest neighbor adaptive density peak clustering analysis with a 1-min step size is applied [26]. Subsequently, scenario analysis is employed to derive the daily power generation plan of the hydropower plant and the set of daily power generation schemes for the unit. Introducing

RO and regional optimization uncertainty transforms the uncertainty of hydropower scheduling decisions into improved inertial weights, culminating in the particle swarm optimization (PSO) algorithm for stepwise optimization—the goal of which is to reduce water usage under various photovoltaic scenarios.

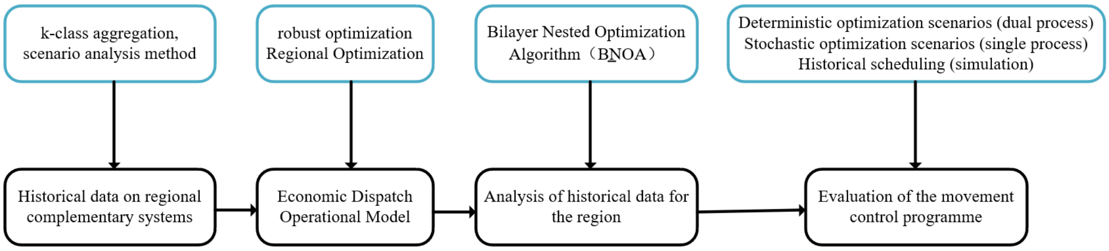

Figure 1. Technology Roadmap for Real-Time-Short-Term Research on Regional Complementary Systems.

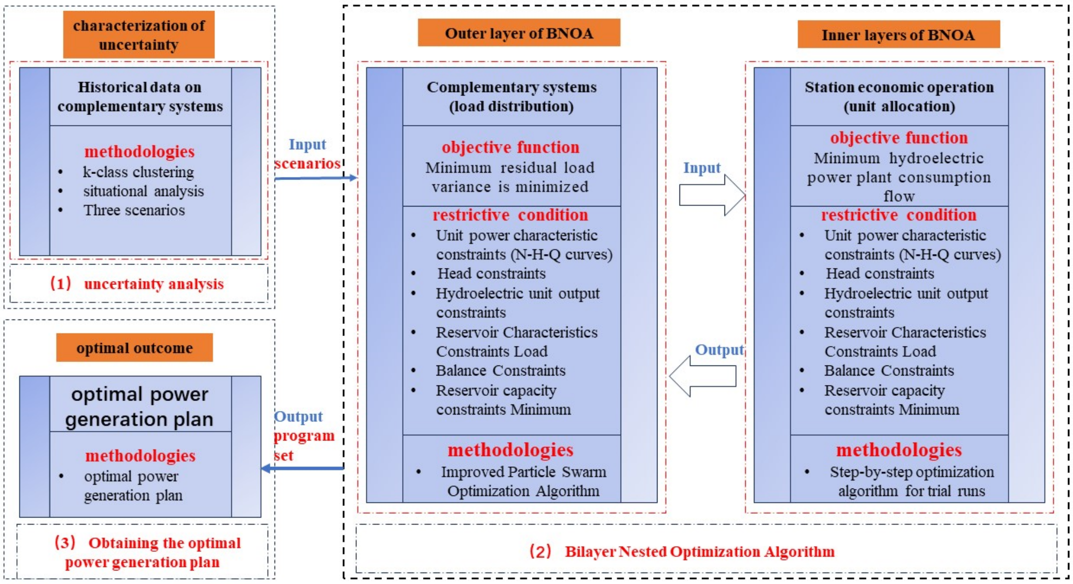

Figure 2. Overall real-time-short-term framework for a regional multi-energy complementary system (MES).

2.2. Economic Scheduling Model Based on Robust Optimization

This study introduces robust optimization (RO), a novel modeling approach for investigating uncertain optimization problems in predicting optoelectronic output to devise a solution applicable to all uncertain input realizations [27–29]. The optimization using the RO algorithm is detailed in the literature [30–33]. Robustness, in this context, signifies the system's ability to maintain performance under external interference conditions. RO is an optimization theory that seeks robust solutions under uncertain conditions, proving especially fitting in situations where uncertain parameters require estimation with associated risks, any realization of uncertainty parameters must satisfy constraints, the objective function or solution is susceptible to model parameter disturbances, and decision-makers cannot bear the significant risks stemming from small probability events. Next, RO is explained based on a simple linear programming problem. Consider the following linear programming model:

$$\max_{x,y}\{a_1x + a_2y\}$$
$$s.t\begin{cases} c_1x + c_2y \le d \\ x, y \ge 0 \\ \forall(c_1, c_2) \in \pi \end{cases}$$

In the formula: x, y are decision variables respectively; c_1 and c_2 are both uncertain parameters; d is a constant; π is a subset of a given set R^2.

2.2.1. Photovoltaic

Figure 3a illustrates the cumulative installed capacity of new PV power plants from 2017 to 2022, while Figure 3b presents the combined installed capacity of centralized and distributed PV power plants during the same period. As illustrated in, the installed capacity of PV power generation is steadily increasing each year globally, with the total projected to reach 328.6 billion kWh by the end of 2022 [34].

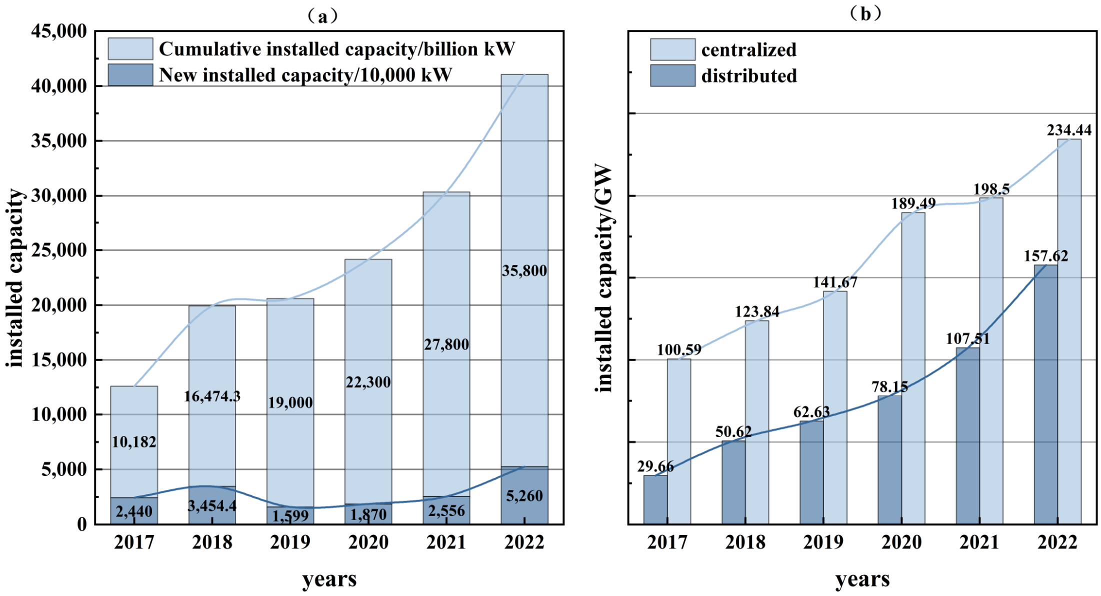

Figure 3. China's Installed PV Capacity, 2017–2022. (**a**): National Cumulative/Newly Installed Capacity; (**b**): Distributed/Centralized PV Installed Newly Installed Capacity [34].

The primary aim of this study is to optimize the real-time and short-term dispatch of regional multi-energy complementary systems, focusing on small power stations characterized by unpredictable and fluctuating output. The study employs multiple scenarios and their associated probabilities to characterize uncertain photovoltaic output. Given that dispatch decisions rely on predictions, the photovoltaic output can be represented by the following Formula (1):

$$P_s = P_f + e \tag{1}$$

where P_s denotes the actual photovoltaic value, and P_f denotes the predicted value obtained through the simulation fitting of historical data from a photovoltaic power station. The photovoltaic prediction error is denoted by e.

Figure 4b displays the historical photoelectric data of the area, and the simulated and fitted model is depicted in Figure 4a as the p_f parameter. The correlation coefficient diagram between this model and each actual curve in Figure 4b is shown in Figure 4c, indicating a minimum R^2 of 93.03%, well above 80%, confirming the excellence of the simulated and fitted model, making it a suitable pf parameter. Assuming the prediction error e follows an unbiased, normal distribution, the study utilizes discrete probability distributions to generate various photovoltaic output scenarios and their corresponding occurrence probabilities. This study considered only three error scenarios to streamline subsequent stochastic planning computations: exceedingly large prediction (e_1), reasonable prediction (e_2), and exceedingly small prediction (e_3). With the probability of the prediction error falling in the interval ($u - 3\sigma$, u + 3σ) being 99.73%, the interval is divided into three equal parts, resulting in three discrete scenarios, as illustrated in Figure 4d. The simulation fitting model is expressed in Equation (2):

$$p_f = \frac{80125.07064}{318.2127\sqrt{2\pi}} \times e^{-\frac{1}{2}\times(\frac{x-809.6072}{318.2721})^2} \tag{2}$$

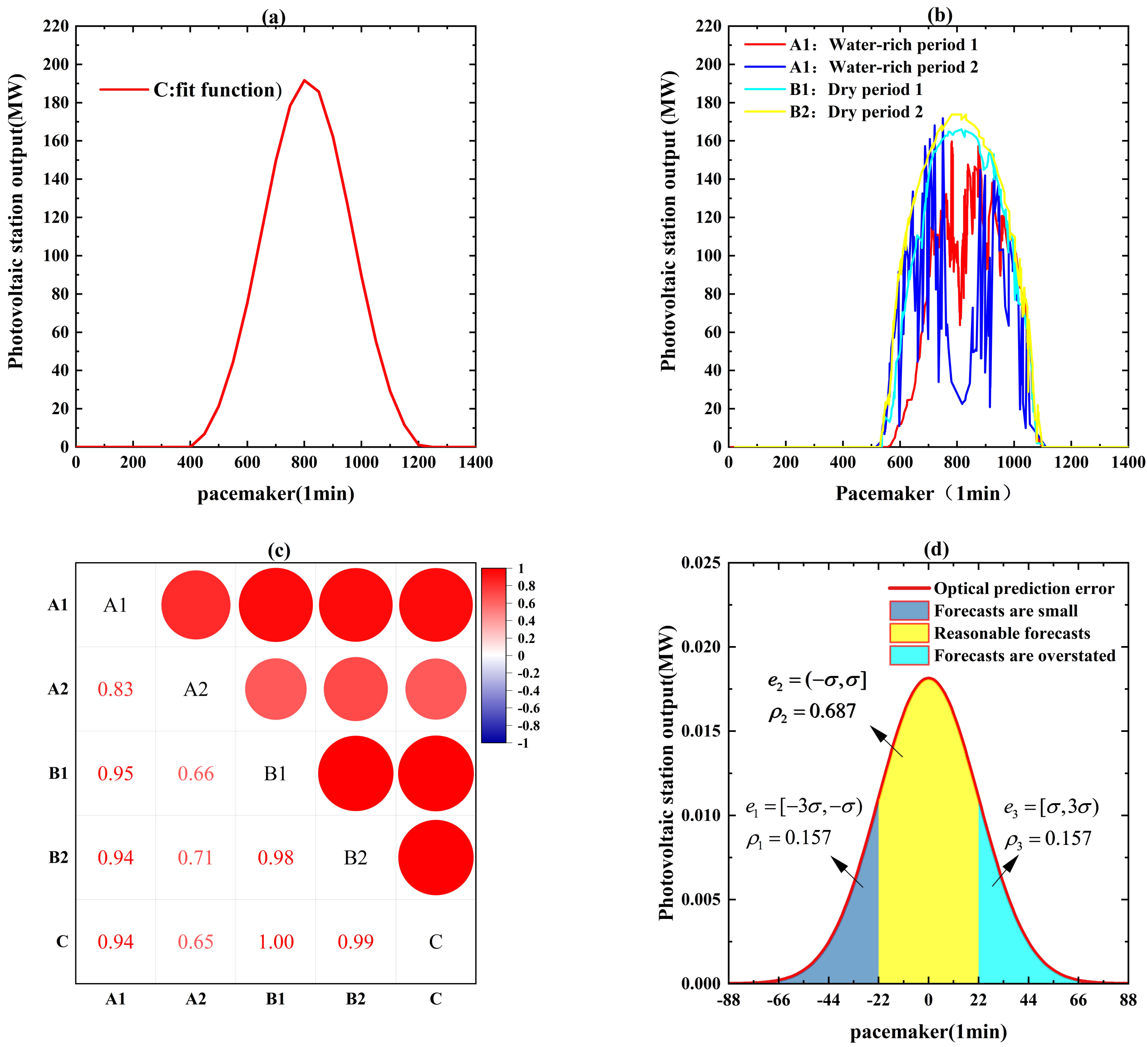

Figure 4. Historical data processing of photovoltaic station output in the region. (**a**): Simulation fitting function for historical data; (**b**): Typical daily data obtained by clustering historical data of the complementary system; (**c**): Heat map showing the correlation coefficient between the fitting function and typical daily data; (**d**): Probability density map of e.

The corresponding probability of occurrence is calculated by integrating the probability density function in each discrete interval [35], as shown in Equation (3):

$$\begin{aligned} \rho_1 &= \int_{\mu-3\sigma}^{\mu-\sigma} f(e)de \\ \rho_2 &= \int_{\mu-\sigma}^{\mu+\sigma} f(e)de \\ \rho_3 &= \int_{\mu+\sigma}^{\mu+3\sigma} f(e)de \end{aligned} \tag{3}$$

where $f(e)$ represents the probability density function of the photovoltaic prediction error; ρ_{11}, ρ_{22}, and ρ_{33} represent the probabilities corresponding to a significant prediction, a reasonable prediction, and a small prediction.

Standardizing the normal distribution of $f(e)$ and the standard normal distribution graph indicates that ρ_1 = 0.1574, ρ_2 = 0.6852, and ρ_3 = 0.1574.

The uncertainty output characterization of a PV plant is then derived and expressed as (4):

$$p_s = p_f + e = p_f = \frac{80125.07064}{318.2127\sqrt{2\pi}} \times e^{-\frac{1}{2}\times(\frac{x-809.6072}{318.2721})^2} + \frac{1}{\sqrt{2\pi}\times 22} \times e^{(-\frac{x^2}{968})} \quad (4)$$

2.2.2. Hydropower Modeling

Objective Function

In addressing the economic dispatch model for hydro-photovoltaic complementary operation, RO is employed to manage the photovoltaic output prediction as an uncertain parameter set characterized by multiple scenarios and their associated likelihoods. The study determines the start/stop state of hydropower units and the load distribution among units to minimize water consumption under various photovoltaic scenarios, accounting for the PV output prediction, incoming runoff prediction, and system-issued load. The objective function is formulated as follows:

$$\min F = \sum\nolimits_{m=1}^{M} \rho_m (\sum\nolimits_{n=1}^{N} \sum\nolimits_{t=1}^{T} \mu_{n,t} r_{m,n,t}) \Delta t \quad (5)$$

where M represents the number of photovoltaic power generation scenarios, M = 3, and m, n, and t represent the photovoltaic power generation scenarios, units, and scheduling period numbers, respectively; F denotes the amount of water consumed by the hydropower plant during the scheduling period; N represents the total number of hydropower units, N = 4; T denotes the number of scheduling periods, T = 24; $r_{m,n,t}$ denotes the amount of flow in the i-th hydropower unit over period t in the m-th photovoltaic scenario; Δt is the stepsize (scheduling period length); and n,t representss the on/off state of the unit; n is a 0–1 variable (1 for unit on, 0 for unit off).

Constraints

The optimization model comprehensively considers 13 types of constraints, predominantly addressing physical limitations related to reservoir and hydropower unit parameters, alongside additional scheduling restrictions.

(a) Crew dynamics limitations

By analyzing and fitting the historical data of the hydropower plant, the N-H-Q curve—representing the operating efficiency curve of a hydropower unit—is derived. As per Equation (6), for units at different heads in small hydropower plants, the operating efficiency varies; for units at the same head, the operating efficiency correlates with the load carried by the unit.

$$r_{m,n,t} = f_{NHQ}(p^h_{m,n,t}, h_{m,t}) \quad (6)$$

where f_{NHQ}(.) represents the functional relationship between the generating flow, output, and head of the unit; $P^h_{m,n,t}$ denotes the hydroelectric unit output; $h_{\mathrm{m,t}}$ represents the generation of clean water head.

During calculations, the overflow flow rate can be directly interpolated based on unit output, headroom, and the N-H-Q curve.

(b) Head constraints

$$h_{m,t} = z^{up}_{m,t} - z^{down}_{m,t} - h^{loss}_{m,t} \forall m, t \quad (7)$$

where $z_{m,t}^{up}$, $z_{m,t}^{dawn}$, $h_{m,t}^{up}$ represent reservoir forewater level, tailwater level, and head loss, respectively.

(c) Reservoir characterization constraints

Reservoir capacity constraints are defined by the water level—reservoir capacity curve and discharge flow—tailwater level curve, expressed as follows:

$$\begin{cases} z_{m,t}^{up} = f_{vz}\left(\frac{v_{m,t}+v_{m,t+1}}{2}\right) \forall m, t \\ z_{m,t}^{down} = f_{qz}\left(\sum_{n=1}^{N} u_{n,t} r_{m,n,t} + WP_{m,t}\right) \forall m, n, t \end{cases} \tag{8}$$

where $f_{v,z}$ denotes the relationship between the front water level and reservoir capacity; $f_{q,z}$ denotes the relationship between the underflow and the tailwater level; $v_{m,t}$ and $v_{m,t+1}$ represent the beginning- and end-reservoir capacities at period t, respectively; $WP_{m,t}$ represents the outgoing flow after deduction of the cited flow for power generation

(d) Hydropower unit output constraints

$$p_n^- \leq p_{\mathrm{m,n,t}}^h \leq p_n^+(h_{\mathrm{m,t}}) \tag{9}$$

These constraints characterize the range of unit output, ensuring it does not fall below a certain minimum value P_n^- , Simultaneously, the unit output must not exceed the maximum output $p_n^+(h_m\ )$, usually related to the head.

(e) Water balance constraints

$$v_{m,t+1} = v_{m,t} + (I_t - \sum_{n=1}^{N} u_{n,t} r_{\mathrm{m,n,t}} - WP_{m,t})\Delta t \tag{10}$$

where $v_{m,t+1}$ and $v_{m,t}$ represent the initial and final storage capacities of the hydropower plant at time t, respectively. I_t represents the average incoming flow for period t.

(f) Hydropower plant flow constraints

$$Q_t^{min} \leq Q_t \leq Q_t^{max} \tag{11}$$

where Q_t^{min}, Q_t^{max}, and Q_t represent the upper and lower limits of the incoming flow and the incoming flow of a small hydropower plant at period t, respectively.

(g) Hydropower plant hydraulic linkage constraints

$$I_{t+1} = Q_t + B_{t+1} \tag{12}$$

where I_{t+1} and B_{t+1} represent the predicted values and error analysis of regional small hydropower plants at time t + 1, respectively.

Given the significance of incoming runoff fluctuations from small hydropower plants in the region, this study introduces interval optimization to establish a deterministic link between the interval incoming runoff in periods t and t + 1.

(h) Reservoir capacity constraints

Characterize the range of variation of the reservoir capacity. The reservoir capacity at each moment must be within a specific permissible range.

$$v^- \leq v_{m,t} \leq v^+ \forall m, t \tag{13}$$

where v^- and v^+ represent the upper and lower limits of hydropower plant capacity, respectively.

(i) Load balancing constraints

These constraints characterize the matching of generation output to load. The sum of the output of the hydroelectric power plant and the output of the photovoltaic power plant is equal to the load requirement issued by the system.

$$\sum_{n=1}^{N} u_{n,t} p_{m,n,t}^{h} + PU_{m,t} = LD_t \tag{14}$$

where LD_t represents the load required for the off-grid grid.

(j) Rotating space constraints

$$\sum_{n=1}^{N} u_{n,t} P_n^{+} - p_{m,n,t}^{h} \geq LR_t \forall m, n, t \tag{15}$$

where LP_t represents the load required for the rotating spare margin.

(k) Constraints on unit output rise and fall

These constraints characterize the speed of increase and decrease in hydroelectric unit output.

$$\left| p_{m,n,t}^{h} - p_{m,n,t-1}^{h} \right| \leq \Delta p \forall m, n, t \tag{16}$$

where Δp denotes the lower limit of the unit speed when the unit is increased/decreased.

(l) Minimum start/stop constraints

These constraints prevent the hydroelectric unit from frequent starting and shutting down. Upon activation, the unit is required to operate continuously for a specified duration before undergoing deactivation. Likewise, upon deactivation, the unit must remain non-operational for a defined interval before being eligible for reactivation.

$$\begin{cases} \sum_{t=1-SU_n+1}^{t} su_{n,k} \leq u_{n,t} \forall \text{n, t} \\ \sum_{t=1-SD_n+1}^{t} sd_{n,k} \leq 1 - u_{n,t} \forall \text{n, t} \end{cases} \tag{17}$$

where k is the time number SU_n and SD_n are the minimum online time and offline time of the unit, respectively; $su_{n,k}$ denotes unit power-on action (1 indicates power-on, and 0 indicates power-off); $sd_{n,k}$ denotes unit power-off action (1 indicates power-off, and 0 indicates power-on).

(m) Restraint of the vibration zone of the unit

When describing the range of permitted output changes under the unit's safe operating conditions, the hydropower unit's output must not be within the vibration zone to prevent mechanical vibration, reducing efficiency and shortening life. The output of the unit must be checked to ensure that it does not lie in the vibration zone.

$$(p_{m,n,t} - p_n^{low})(p_{m,n,t} - p_n^{up}) \geq 0 \ \ \forall m, n, t \tag{18}$$

where p_n^{up} and p_n^{low} represent the upper and lower limits of the vibration zone of the unit, respectively.

2.3. Double-Level Nested Optimization Algorithm Based on Economic Dispatching Model

Robust optimal economic dispatch models encompass a multitude of linear and nonlinear constraints, ranging from vibration zone limits to time-interval coupling constraints and minimum start/stop constraints. The objective of this study is to decompose intricate problems into smaller interconnected sub-problems, resolved within the same framework using a double-level nested optimization technique. In other words, the scheduling challenge in the domain of real-time and short-term scheduling of multi-energy complementarity comprises three interlinked sub-problems: (1) characterizing uncertainty in renewable energy outputs like wind and light; (2) modeling scheduling with coupled uncertainties;

and (3) devising an efficient and reliable scheduling model solution. The bi-level nested algorithm optimization process is illustrated in Figure 5.

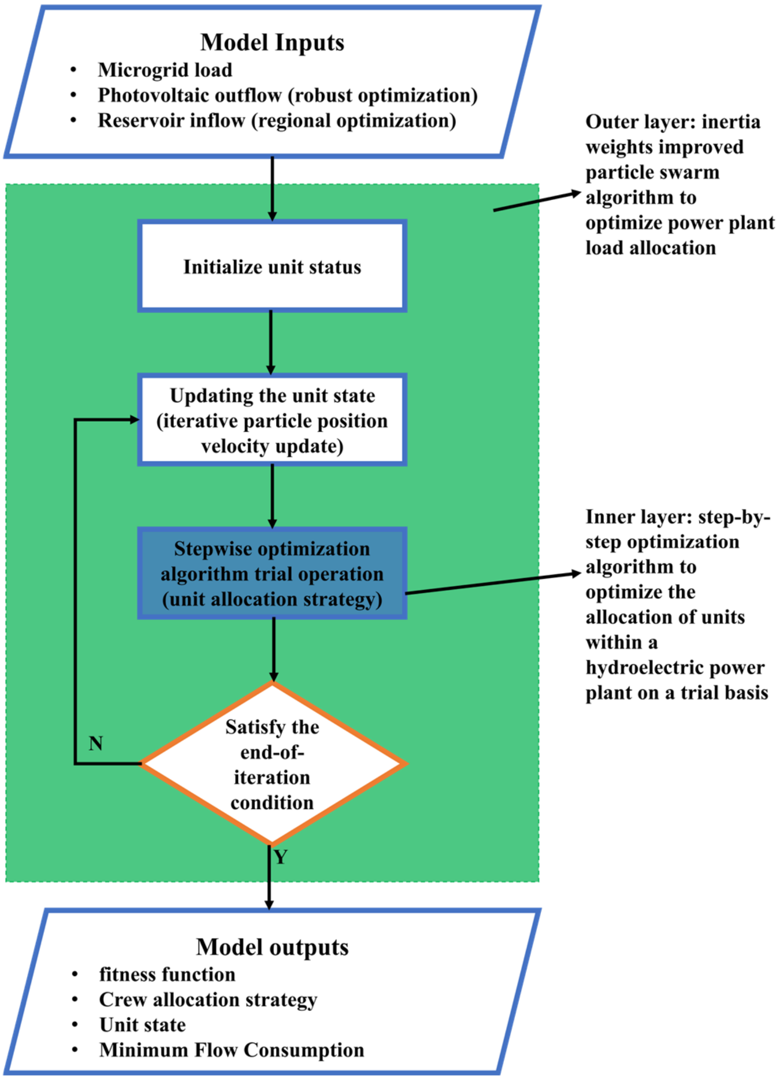

Figure 5. Optimization Model for Bi-Level Nested Algorithms.

2.3.1. Outer Layer Optimization (Economic Operation Modeling to Address the "Electricity to Water" Problem)

The study focuses on a small hydroelectric power plant, a photovoltaic power plant, and a microgrid complementing system in the region. Given the area's high runoff variability, the influence of synergistic energy system optimization cannot be overlooked. The outer layer method in this study employs inertia weights to enhance the PSO algorithm and allocates the power station's load based on peak shaving, aiming to minimize the variance of the remaining load as the goal function. Inertia weights, first proposed by Shi and Eberhart, measure a particle's ability to adopt the velocity of its precursor. Larger inertia weights correspond to better global and poorer local search, while smaller inertia weights correspond to better local and poorer global search.

PSO is a meta-inspired swarm intelligent optimization algorithm where each particle explores a D-dimensional space and possesses position vectors $x = [x_1, x_2 \ldots x_n]$ and the velocity vector $v = [v_1, v_2 \ldots v_n]$. Additionally, each particle has a memory function. The population's global optimal particle location is $P = [P_{i1}, P_{i2} \ldots P_{id}]$, and the historical optimal particle position of the ith particle is $G = [G_1, G_2 \ldots G_3]$. Each particle progresses toward the current optimal particle position in the solution space while iteratively updating its position and velocity vectors using Equation (18).

$$v_i^d(t+1) = wv_i^d(t) + c_1r_1(p_i^d(t) - x_i^d(t)) + c_2r_2(G^d - x_i^d(t)) \quad (19)$$

$$x_i^d(t+1) = x_i^d(t) + v_i^d(t+1) \quad (20)$$

where I = 1, 2,. . .N representing the number of particles, with N = 400 in this study; c_1 and c_2 represent the self and population learning factors, respectively; r_1 and r_2 are random numbers in the interval [0, 1]; v_i represents the velocity of the i-th particle; and w denotes the inertia weight represented by the inertia vector of the particle population.

Innovative points:

(1) A recorder is introduced to the original model to distribute initial particles uniformly in space D rather than having random particle positions, effectively preventing optimization from falling into local optima.

(2) To balance the global exploration and local development ability of PSO, this study proposes an improved PSO algorithm with inertia weights. It transforms the linearly decreasing variable of inertia weights into a nonlinear inertia weight, as depicted in Figure 6.

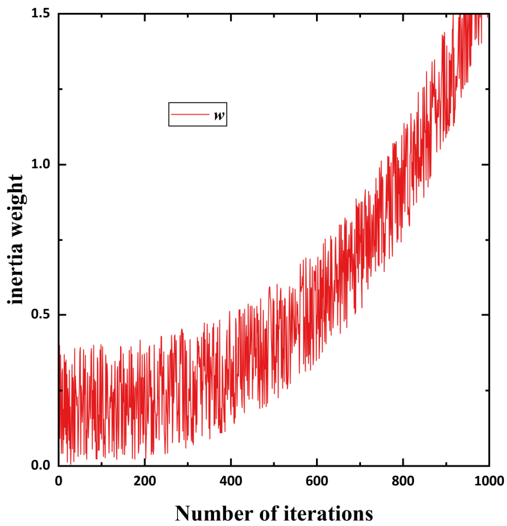

Figure 6. Nonlinear inertial weights 1000 iterations.

The improved inertia weights are expressed in the following equation:

$$w = rw_{min} + (w_{max} - w_{min})((e^{\frac{t}{T}} - 1)^2) \quad (21)$$

where r denotes a random number in the interval [0, 1]; w_{min} and w_{max} represent the minimum and maximum values of w, respectively, and w_{min} = 0.3; t is the number of current iterations; and T is the maximum number of iterations.

In Figure 6, the inertia weight (ω) is determined through a nonlinear incremental distribution approach, causing substantial fluctuations throughout the entire iteration process. This method not only amplifies local search capabilities in the initial stages but also fortifies global search capabilities in later iterations. Moreover, the nonlinear inertia weight method exhibits superior fitting and simulation capabilities, leading to enhanced convergence speed and global convergence compared with linear inertia weight and fixed-value inertia weight methods. The essential steps of the enhanced PSO approach with outer inertia weights are illustrated in Figure 7.

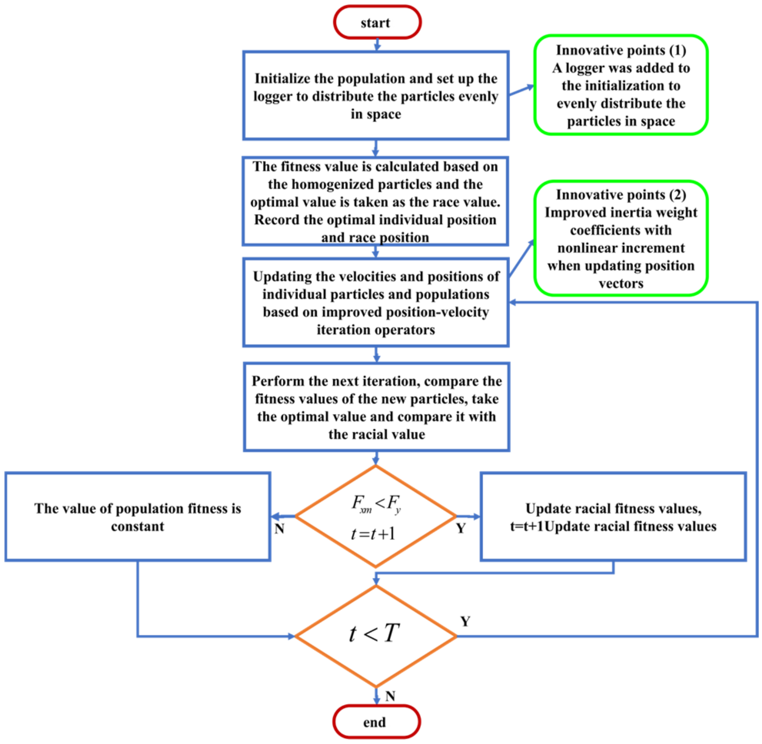

Figure 7. Outer layer: inertia weights improved particle swarm optimization algorithm flowchart.

2.3.2. Inner Layer Optimisation (Optimisation of Hydroelectric Units)

Hydroelectric Power Plant Output Scenarios and Time Sequences

Forecasting runoff volume and obtaining the overall power plant production forecast results are prerequisites for introducing the regional optimization method [36–38]. The scenarios of hydropower plant output and the temporal fluctuation of output during the scheduling cycle are as follows. The daily fluctuation distribution pattern of the hydropower plant in each period is derived from historical data of a hydropower plant in Southwest China.

$$\begin{aligned} HP^n &= (HP_0^n, HP_1^n, HP_2^n \ldots HP_{\mathrm{T}}^n) \\ \Delta hp_t^n &= hp_{t+1}^n - hp_t^n \end{aligned} \tag{22}$$

where $HP_t^n$and HP_t^n denote the output and output fluctuation at the cycle in the $\mathrm{n_{th}}$ sample scenario, respectively.

The fluctuations of all samples for step size t can be expressed as follows:

$$\Delta HP_t = (\Delta hp_t^1, \Delta hp_t^2, \ldots \Delta hp_t^n) \tag{23}$$

where n is the set of scenes.

The temporal fluctuation of hydropower plants is discerned by analyzing the frequency of all data. Figure 8 displays the time fluctuations of hydropower plants across various confidence levels, with the first three intervals selected to illustrate these fluctuations. The frequencies of the fluctuating intervals of hydropower plant production, ordered from largest to smallest, can be expressed using Equation (23).

$$(f_t^0, f_t^1, \ldots f_t^m \ldots, f_t^M) \tag{24}$$

where $f_t^0 > f_t^1 > \ldots > f_t^m > \ldots > f_t^M$. f_t^0 denotes the frequency of the m-th fluctuation interval in time t. f_t^0, f_t^1, and f_t^2 denote the frequencies of $\left(\Delta hp_t^{k_0},\ \Delta hp_t^{k_0}\right]$, $\left(\Delta hp_t^{k_1},\ \Delta hp_t^{k_2}\right]$,

$\left(\Delta hp_t^{k_2}, \Delta hp_t^{k_3}\right]$ respectively. As shown in Figure 9. Confidence intervals at different confidence levels can be given by Equation (24):

$$\begin{cases} f_0 = f_t^0 & \rightarrow (\Delta hp_t^{k_0}, \Delta hp_t^{k_1}] \\ f_1 = f_t^0 + f_t^1 & \rightarrow (\Delta hp_t^{k_1}, \Delta hp_t^{k_2}] \\ f_2 = f_t^0 + f_t^1 + f_t^2 & \rightarrow (\Delta hp_t^{k_2}, \Delta hp_t^{k_3}] \end{cases} \tag{25}$$

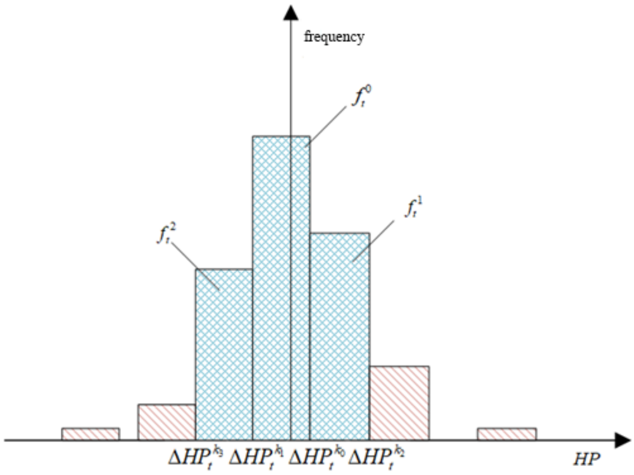

Figure 8. The first three intervals serve as temporal fluctuations of the hydroelectric plant at different confidence levels.

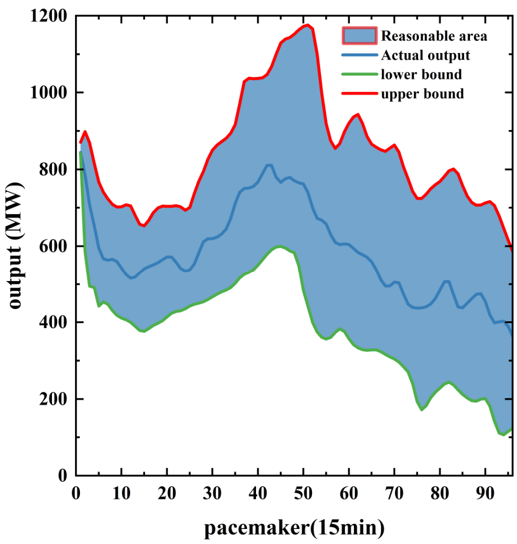

Figure 9. Characterization of uncertainty after optimization of hydroelectric power plant output region.

The expected scenarios for hydropower plant output are derived through clustering historical data, utilizing the confidence level to ascertain uncertainty. Uncertainty characterization for hydropower plant output is represented by Equation (25):

$$\begin{gathered} HP^e = (hp_0^e, hp_1^e, \ldots, hp_t^e, \ldots, hp_T^e) \\ \begin{cases} hp_0^{up} = hp_0^e \\ hp_t^{up} = hp_{t-1}^{up} + \Delta hp_t^{k_3} \end{cases} \\ \begin{cases} HP_t^{up} = (hp_0^{up}, hp_1^{up}, \ldots, hp_t^{up}, \ldots, hp_T^{up}) \\ HP_t^{low} = (hp_0^{low}, hp_1^{low}, \ldots, hp_t^{low}, \ldots, hp_T^{low}) \end{cases} \end{gathered} \tag{26}$$

where HP^e denotes the set of desired hydropower plant output scenarios; HP_t^{up} and $upHup$ denote the upper and lower boundary values of the hydropower plant output with stepsize t and uncertainty, as depicted in Figure 9.

$$Q_t = \min \sum_{j}^{J} q_{j,t} \tag{27}$$

where Q_t denotes the water consumption in stepsize t of the hydropower plant, and $q_{j,t}$ represents the water consumption of the j_{th} unit in the stepsize of the hydropower plant.

The Inner-Layer Optimization Models for Hydroelectric Power Plants Incorporate Specific Strategies

(1) The inner layer optimizes the load distribution strategy across units using SOAT Operational. Unit load distribution is modeled with a stepwise optimization algorithm (SOA), treating each unit as a stage, and the input unit number represents the stage variable (d = 1, 2,. . ., N) for the facing stage of the residual phase. The output after the stage can be considered the unit's overall output. Consequently, the state transfer equation of the SOA model is as follows:

$$\sum_{j=1}^{d} p_{j,t} = \sum_{j=1}^{d-1} p_{j,t} + p_{d,t} \tag{28}$$

Style: $\sum_{j=1}^{d} p_{j,t}$ is the total output of the 1st~dth unit.

(2) When considering hydropower units, the unit on/off state variable (us) constitutes a two-dimensional coding, altering the conventional coding strategy of optimizing only the number of units. This change involves optimizing the time nodes and the number of units when the hydropower unit models are not the same as signified by:

$$\begin{bmatrix} us_{1,1} & \cdots & us_{1,T} \\ \vdots & \ddots & \vdots \\ us_{N,1} & \cdots & us_{N,T} \end{bmatrix} \tag{29}$$

The total number of optimization variables in the algorithm is NT. When the hydropower plant units are of the same type, the optimized unit state must be simplified to maximize the number of online units. In this case, there are T optimization variables, and the solution comprises the following components:

$$U = [ou_1, ou_2, \cdots, ou_T] \tag{30}$$

where ou_1, ou_2, . . ., and ou_T represent the online units in each scheduling period during the entire T period. The number of online units in each T scheduling period is the number of online units in each scheduling period.

To prevent frequent startup and shutdown of units, the number of turned-on units in two adjacent time steps remains constant during that time step. The number of time nodes is denoted by (so-1), the number of optimization variables is denoted by (so-1), the number of optimization variables is denoted by (2 × so-1), and the sum of the sequentially unchanged unit start-ups throughout the scheduling period is denoted by so. When the number of stable operation periods is so = 5, the number of optimization variables for two-dimensional coding is only 9, significantly reducing the difficulty of optimization solving. Using hydropower plant daily scheduling as an example, with a scheduling duration of 15 min, the number of optimization variables for traditional unit coding is 96. According to Figure 10:

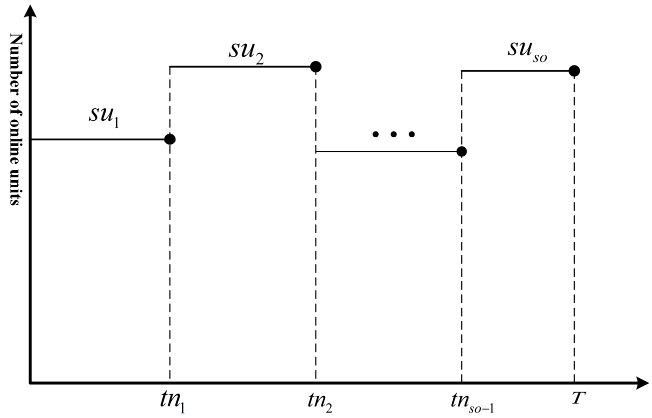

Figure 10. Continuous processing on/off two-dimensional coding schematic.

Two-dimensional encoding was used to solve Equation (30):

$$U = [tn_1, tn_2, \cdots, tn_{so-1}, su_1, su_2, \cdots, su_{so}] \quad (31)$$

where $tn_1, tn_2, \ldots, tn_{so-1}$ denote the time nodes at which the state of the unit almost changes; $su_1, su_1, \ldots, su_{so}$ indicates the number of online units for each stable operation period.

(3) The load factor η_i of the hydropower plant is calculated, linking to the planned daily power generation E_i^c and the maximum output of the hydropower plant, P_i^{max}:

$$\eta_i = \frac{(E_i^c / T)}{P_i^{\max}} \quad (32)$$

The deviation value ΔQ_i of water consumption in the power station transforms the original station unit load allocation model to the station unit multi-scenario model. The enhanced model is depicted in Figure 11.

$$Q_t = \Delta Q + \min \sum_{j=1}^{J} q_{j,t} \quad (33)$$

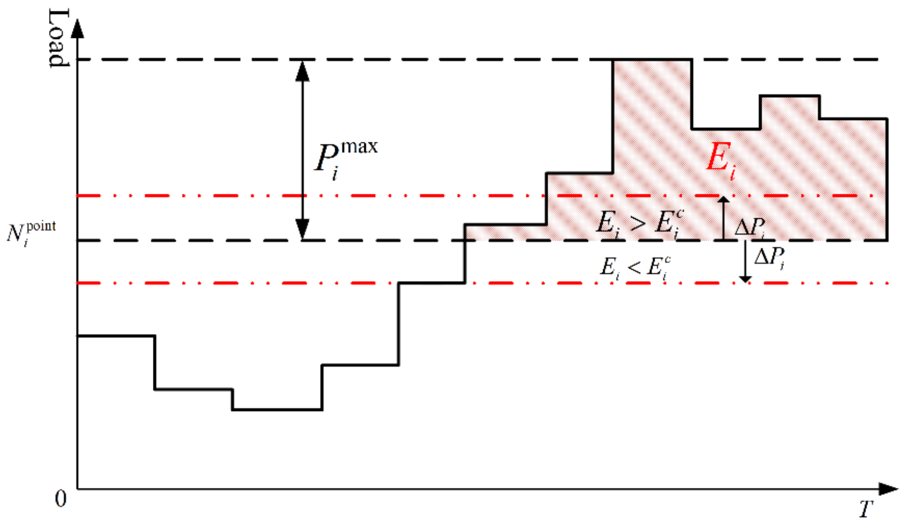

Figure 11. Schematic diagram of the cutting process.

(4) The objective function of the unit combination model is established following the Bellman optimization principle. The recursive form, as shown in Equation (33), is employed:

$$R^*_{d,t}(\sum_{c=1}^{d} p_{c,t}) = \min\left\{f_{rph}(p_{d,t}, h_t) + R^*_{d-1,t}(\sum_{c=1}^{d} p_{c,t} - p_{d,t})\right\} \quad (34)$$

where $R^*_{d,t}\left(\sum_{c=1}^{d} p_{c,t}\right)$ denotes the optimal water consumption flow rate when the total output $\sum_{c=1}^{d} p_{c,t}$ is distributed between units $1 \sim d. f_{rph}(p_{d,t}, h_t)$ denotes the water consumption flow rate of power generation in unit d when the net load is d when the net load is $p_{d,t}$, and the net header of water is h_t.

Trial Operational

The preceding step-by-step optimization algorithm model solely determines the unit's load allocation strategy within one time period, as depicted in Figure 12. When addressing the load allocation challenge across multiple periods, resolution is sought through the trial algorithm. The fundamental steps of the trial algorithm are outlined as follows:

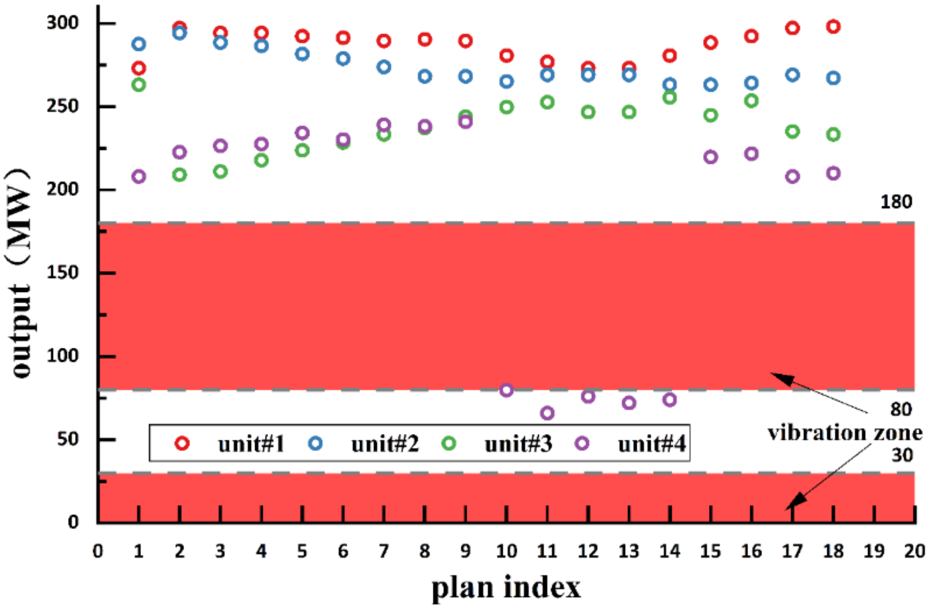

Figure 12. Expected incoming flows at the 83% confidence probability level for the hydroelectric power plant's 33rd hour of trial calculations in the multi-generation program.

Step one: Initial values for runoff Q_t and generation referral flow q_t are determined based on the hydropower plant's output characteristics graph and the provided initial water level/reserve after the outer layer optimization. The daily planned generation load is subtracted as the initial output of the hydropower plant optimized in the inner layer, representing the target output to be achieved by each unit's combination.

Step two: The load distribution strategy among the units is determined using a step-by-step optimization method, as illustrated in Figure 13. This process identifies the optimal flow consumption along with the matching number of units and codes.

Step Three: Figure 14 illustrates the flow of determining whether the unit code corresponding to q_{trm} and the corresponding output of each unit satisfy the prohibited operation area constraint (17) and the minimum start-stop constraint (16). If the results are positive, the process stops, and the optimal generation flow is acquired, leading to the calculation of the end water level/reservoir capacity entering the optimization plan for the period. If not, the process is reiterated until both constraints are fulfilled.

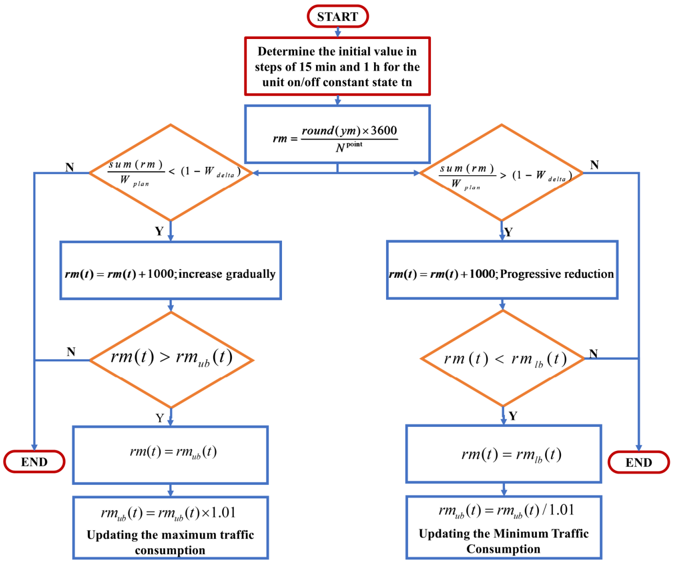

Figure 13. Inner layer: step-by-step optimization algorithm trial operation flowchart.

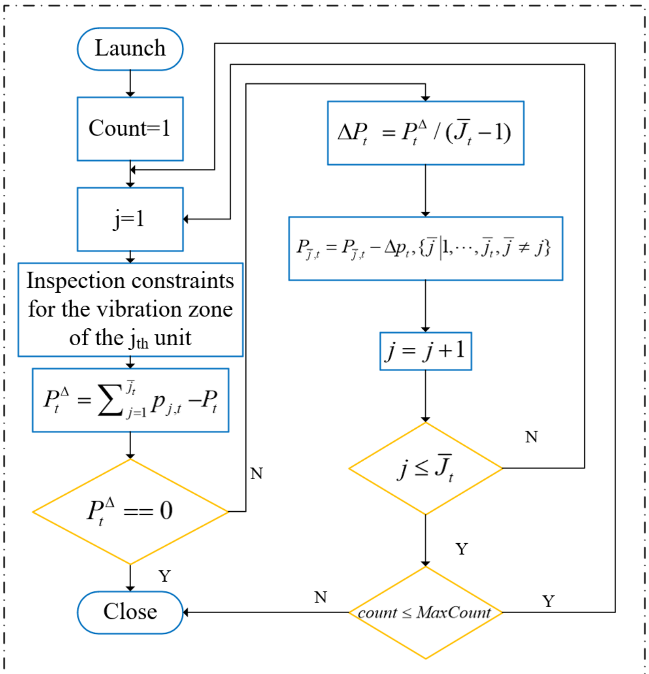

Figure 14. Flow chart for vibration zone restraint inspection.

3. Case Studies

3.1. Partial Parameterization of the Power Station and Multi-Scenario Settings

During the examination of a typical day in June 2016, the operational data of the river power plant in the specified area was scrutinized. The plant was initiated with a water level of 191.02 m and a power requirement of 3677.5 MW. Other relevant data encompassed:

1. River hydro units (UNIT#1–4) output sequence from 1 March 2016 to 31 March 2016, at a 1-h resolution.
2. Sequence of PV output from PV power plants in the region spanning 1 April 2013 to 1 April 2014, with a 15-min resolution.
3. Output sequence on 15 June 2016, at a 1-min resolution for the water-photovoltaic (WPV) power plants in the region, consisting of 1200 MW of hydropower and 200 MW of photovoltaics.

4. Reservoir inflow runoff sequence from January 1956 to December 2011 at a monthly resolution.

Specific transformations and processing techniques were applied to standardize the sequence length and time resolution of the data. This resulted in an input model for the economic operation of the power plant, including load, photovoltaic output, and reservoir inflow, all with a 1-h resolution. The simulation period considered was 1 month. Figure 15 illustrates the load box diagram of the multi-energy complementary system in the area after technical processing and time alignment, representing the input data for economic operation simulation.

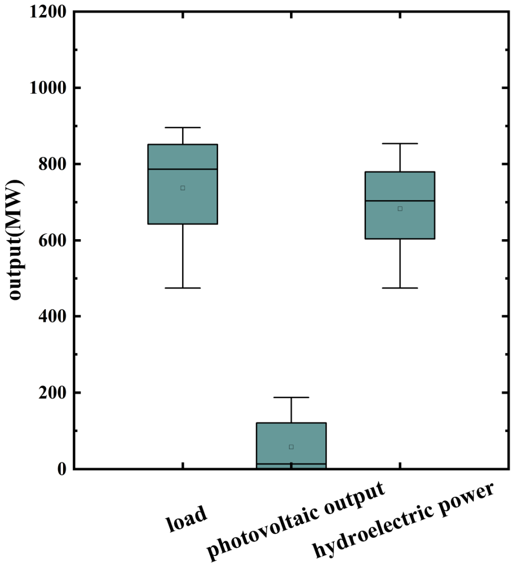

Figure 15. Box plot of microgrid complementary system output on a typical day in June.

Daily optimization calculations were performed using photovoltaic output and load data from 15 June 2016, to address the economic operation problem, as shown in Figure 16. The scheduling period was set at 15 min, covering a total scheduling time of 1 day.

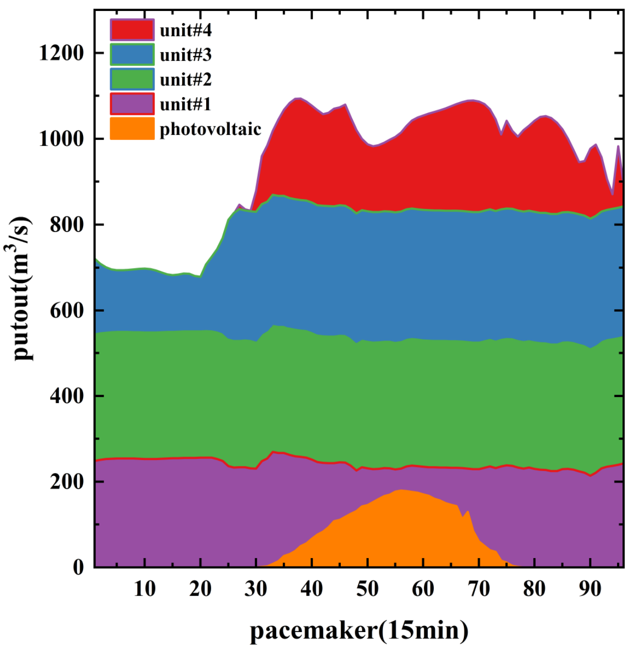

Figure 16. Typical June historical dispatch (simulation) for the region’s multi-energy complementary systems.

3.2. Program Parameter Design

The standard daily optimal scheduling computation for a regional multi-energy complementary system utilizes a step size of t = 15 min, a total scheduling duration of T = 1 d = 24 h, and a scheduling node of s = T/t = 96. Three distinct scenarios were established: a historical scheduling scenario (simulation), a deterministic optimal scheduling scenario (single-process, two-tiered optimization nested), and a stochastic optimal scheduling scenario (multi-process, two-tiered optimization nested). The distinction between the stochastic and deterministic scenarios lies in the prediction of PV generation and runoff. Table 1 below shows the basic data of the river power station.

Table 1. Selected data on hydroelectric power stations.

Power Plant	Regulating Capacity	Installed Capacity (MW)	Normal/Dead Water Level (m)	Maxi/Min Discharge (m^3/s)	Max/Min Head (m)	Unit Vibration Limit (MW)
power plants	year	300 × 4	200/161.2	340 × 4/0	121.5/80.7	(0–30) U (80, 180)

The inertia weight-improved PSO algorithm, with 400 populations and a maximum of 1000 iterations, was employed as the outer layer, while the inner layer of the daily optimal scheduling computation followed a SOA. Table 2 provides details on the trial operational and 2D coding parameters, alongside the number of stable operation periods *so* = 6 to adhere to minimal on/off constraints.

Table 2. Economic dispatch model operating parameters.

Parameter Category	Symbol	Value	Unit
Min. start-up time	SU_n	1	[h]
Min. stopping time	SD_n	1	[h]
Climbing speed of output	Δp	10	[MW/s]
Spinning reserve	LR_t	80	[MW]
Vibration zone upper limit	p_j^{up}	30.180	[MW]
The lower limit of the vibration zone	p_j^{up}	0.80	[MW]
The upper limit of unit output	p_n^+	0	[MW]
The lower limit of the unit	p_n^-	300	[MW]

3.3. Effectiveness Analysis of Double Nested Algorithms

Deterministic scenarios were considered for optimization to examine the effectiveness of the double-layer nested algorithm model in the economic operating characteristics of complementary systems. In the deterministic scenario, the output uncertainty of the power station was perfectly predicted. Figure 17 depicts the operating efficiency curve of the unit under different water heads in this scenario. As shown in Figure 17a, the operating efficiency of a single hydropower unit generally increases within a specific range as the load increases. However, increasing the number of units turned on decreases operating efficiency and increases flow consumption, implying an overall decrease in power station efficiency. Figure 17b illustrates that a higher water head reduces flow consumption and enhances operating efficiency for the same unit and number of units started. Consequently, increasing the power generation head and reducing the number of units in a hydropower station have significant implications for economical operation.

Figure 18 presents the typical daily optimization process of the HPV system in the region, highlighting enhanced stability in the remaining load of the power grid compared with actual operation. The residual standard deviation, an index post-optimization, is 856.48 MW, surpassing the actual operation value of 1080.15 MW, indicating a notable peak-shaving effect achieved through this method. Additionally, the daily dispatch plan of the hydropower station is executed based on the remaining load of the power grid, considering both the mitigation of microgrid fluctuations and the characteristics of wind power. This model proves effective in deterministic scenarios, showcasing superior performance compared with actual operation. The power generation plan derived from optimization demonstrates commendable peak-shaving performance and higher energy storage value in uncertainty scenarios, reinforcing the practical significance and economic viability of the proposed approach.

The subsequent program is independently run 20 times using MATLAB statistics. Each run aims to find optimal results within 5 min, demonstrating the computational efficiency post-dimensionality reduction and the balance between accuracy and efficiency. Figure 19 illustrates the number of two-dimensional coding variables for unit 11, encompassing 5 time nodes and 6 h of stable scheduling. The initial solution is derived from the two-dimensional encoding in the early stages of optimization, generating a random number of units that do not reach the optimal state. The improved PSO algorithm, dividing particles uniformly in space during the initial solution, converges smoothly in subsequent iterations. As depicted in Figure 19a, convergence is achieved in a maximum of 56 iterations, attaining 573 m^3/s due to improved Weight Coefficients. After 51 iterations and 20 statistical runs, the optimal flow rate stabilizes at 573 m^3/s, indicating stable and convergent optimization results. Compared to the actual scheduling of 585.6 m^3/s, water consumption decreases by 2.2% after optimal scheduling.

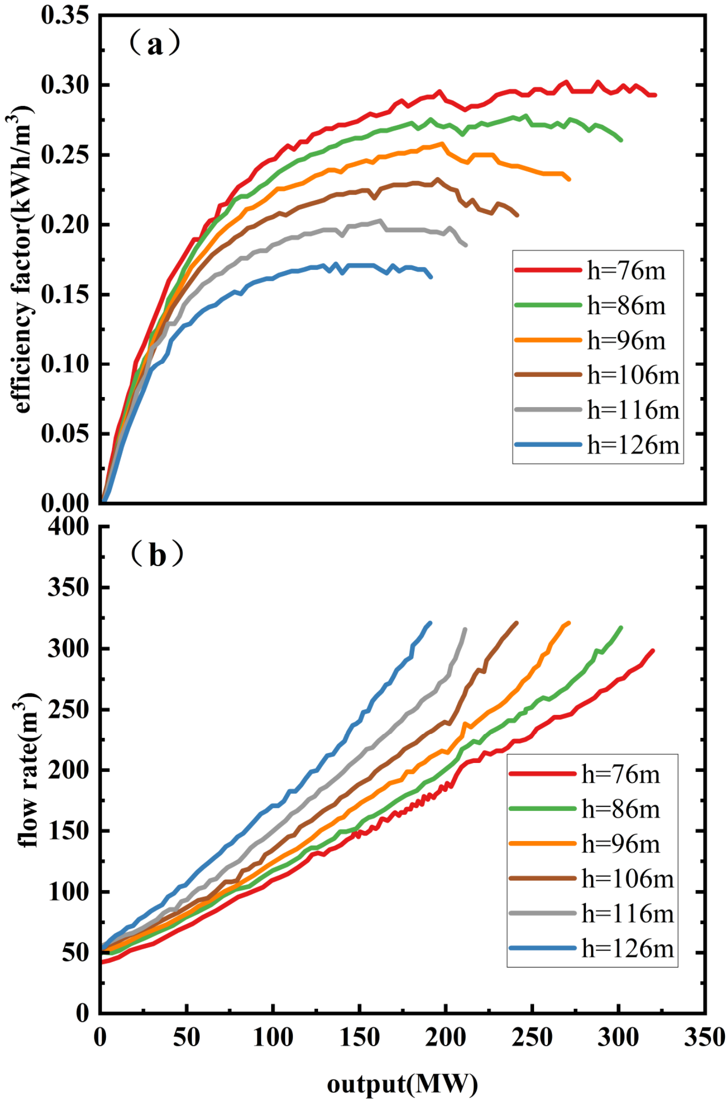

Figure 17. Graphs of unit efficiency curves at different heads: (**a**) unit efficiency versus output; (**b**) unit consumption flow versus output (Unit efficiency: electricity that can be generated per unit cubic meter of water).

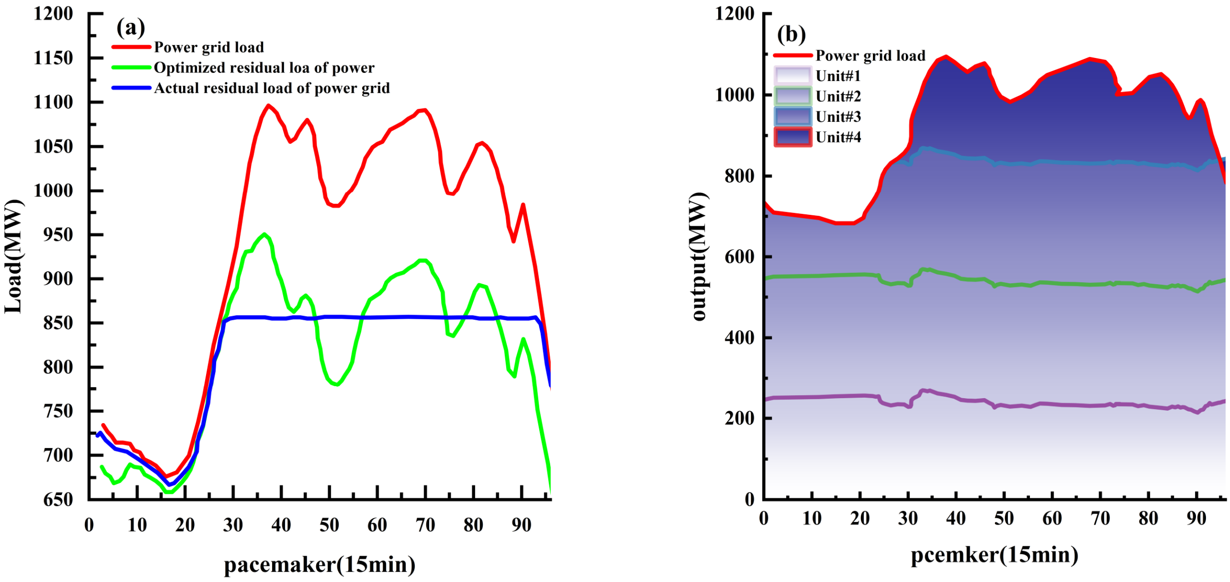

Figure 18. (**a**) Residual load process of the microgrid in the region; (**b**) Uncertainty characterization of the generation of each hydropower plant after regional optimization.

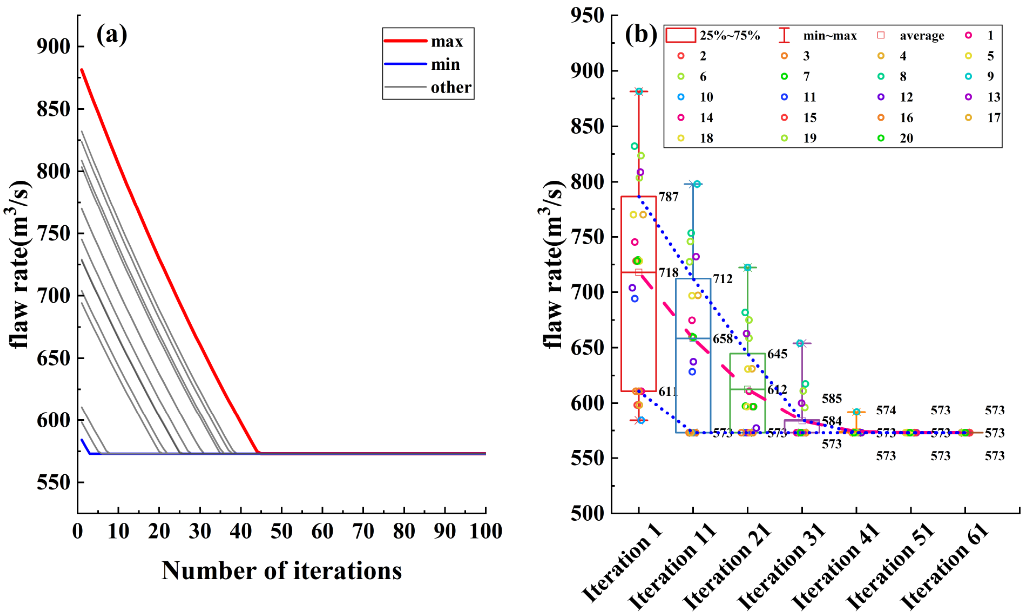

Figure 19. Statistical graphs of twenty results for a typical day of optimization by the two-layer nested optimization algorithm: (**a**) Iteration count and flow rate consumption optimization relationship; (**b**) Iteration count and flow rate consumption box plots.

The unit's continuous start-stop and vibration zone requirements render the stepwise optimization approach challenging. This approach handles load distribution over only one time period, making it difficult to meet the requirements. The particle swarm intelligent optimization approach alone may struggle due to the study's 384 optimization variables and numerous nonlinear constraints. In conclusion, the double-layer nested method proposed in this study combines the potent nonlinear processing of stepwise optimization with the parallel search capabilities of the intelligent algorithm, effectively addressing the unit combination problem.

A crucial parameter for balancing the stability and economy of power plant operation in the two-layer nested algorithm is the number of stable operation periods (*so*). As units are started and stopped more frequently, *so* increases, leading to less stable power plant operation. Figure 20 illustrates the average flow consumption and error for various numbers of steady operation periods (*so*), demonstrating how this parameter affects the hydropower plant's economic performance. The average flow rate is higher with smaller *so* values; as *so* increases, the average flow rate gradually decreases, reaching its minimum at *so* = 7. Further increases in *so* enhance the average flow rate and broaden the error range, resulting in lower optimization outcome stability. Smaller *so* values make unit start/stop requirements easier to satisfy but reduce flexibility and increase flow consumption. The algorithm, equipped with a penalty function for minimum on/off constraints, adjusts the average flow rate based on this function's impact. Synthesizing this parameter must be performed practically, using a trial algorithm based on minimum on/off constraints.

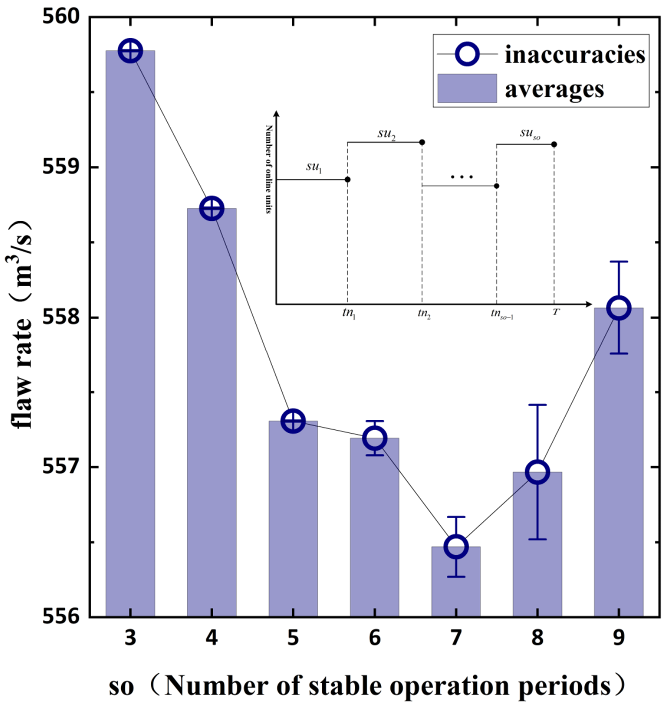

Figure 20. *So* in the economic timeframe of operation.

4. Comparison of Three Dispatch Scenarios for Individual Cases

Because of geographical and climatic factors, solar and wind energy in China are primarily concentrated in the northwest and southwest regions, alongside hydropower [39]. This study utilizes the water-optical synergistic optimization system tailored to the characteristics of the Southwest China plateau region, which is abundant in solar and water resources but relatively lacking in wind energy, with an installed hydropower capacity of approximately 10,000 MW. Additionally, the average annual solar radiation surpasses 6381 MJ/m^2, with more than 2719 h of sunshine annually and a sunshine percentage between 55% and 80%, signifying ample solar energy resources (Figure 21) [40]. Characteristics include microgrids, small power stations, and significant load (runoff) fluctuations.

In this study, a multi-energy complementary system in the area serves as a case study for deterministic optimal scheduling (single process) and stochastic optimal scheduling (dual process, trial operation). The program runs independently 20 times, and optimization results are statistically presented in Table 3. These results are then compared with historical scheduling (simulation) to scrutinize variations between historical scheduling scenarios, stochastic scheduling, and deterministic scheduling.

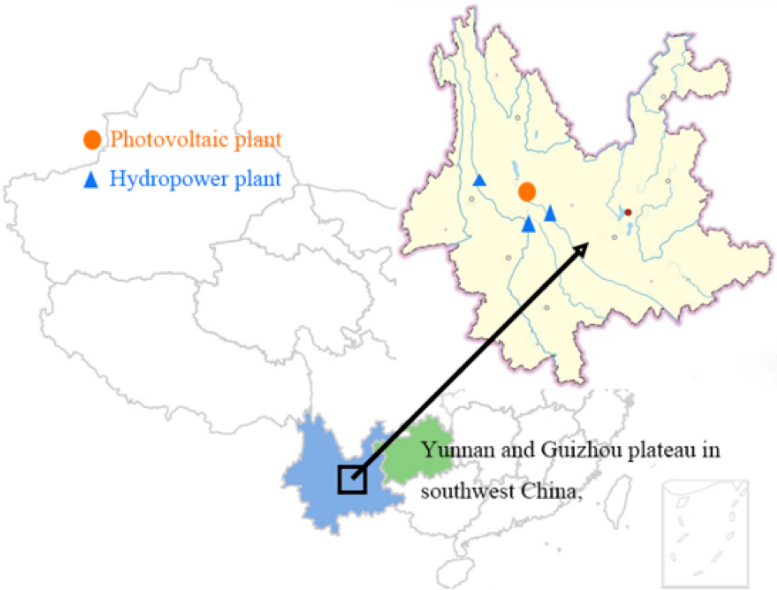

Figure 21. Topographic map of the study area.

Table 3. Statistical results of 20 deterministic and stochastic optimizations in the region on a typical day in June 2016.

Statistical Counts	Deterministic Optimization	Stochastic Optimization
1	572.6	574.1
2	572.7	574.6
3	572.6	574.1
4	573.1	574.6
5	572.5	574.5
6	572.4	574.7
7	572.1	574.2
8	572.8	574.9
9	573.4	573.3
10	573.8	574.9
11	573.4	574.4
12	573.8	575.0
13	572.6	573.1
14	573.2	574.1
15	572.9	574.6
16	573.0	573.1
17	572.4	573.3
18	572.5	574.0
19	572.8	574.3
20	572.3	574.7
average	572.8	574.2
statistics	0.5	0.6
average ± statistics	572.8 ± 0.5	574.2 ± 0.6

As indicated by the data in Table 3, every deterministic optimization scenario exhibits lower average flow consumption than the stochastic optimization scenario. This outcome ensures adherence to load balancing constraints in all PV output scenarios (overpredicted, reasonably forecasted, and underpredicted). In the stochastic optimization scenario, the number of online units is an adaptable optimization variable, ensuring the complementary system's reliability even in the event of inaccurate PV predictions. However, the system's economic efficiency is compromised because decision-making incorporates the worst-case scenario (Economic scheduling model based on RO), leading to higher costs.

Figure 22 illustrates a declining trend in reservoir levels for all three scheduling situations. A comparison of the end levels among different scheduling methods reveals that the historical scheduling scheme has the lowest end level, the stochastic optimization scheme exhibits a reasonably high-end level, and the deterministic optimization strategy exhibits the highest end-reservoir level. This indicates that both optimization scenarios enhance water use efficiency while reducing the water required for electricity production. In contrast to the deterministic scheduling scheme, the stochastic scheduling scheme introduces RO, resulting in more cautious decision-making and consequently saving less water. The chart also depicts the growth of cumulative water savings for the two optimal scheduling systems, attributable to the optimization scheme within rotating standby and vibration zone constraints, causing the number of hydropower plant start-ups in specific periods to fluctuate rapidly, along with water consumption.

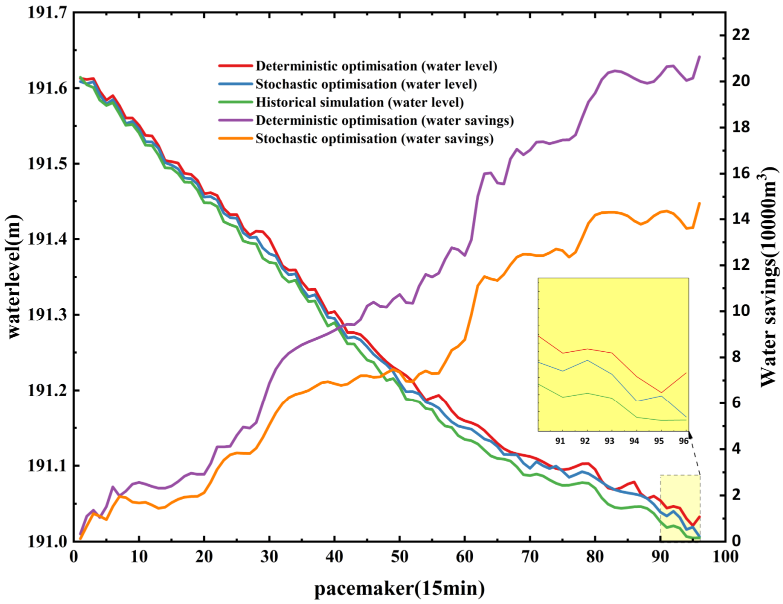

Figure 22. Reservoir Levels and Water Savings on Typical Days for Different Dispatch Scenarios. In calculating water savings for the two optimization scenarios, the simulated dispatch scenario (historical dispatch scenario for a typical day) is the baseline.

Table 4 compares overall water consumption, the probability of non-vibrating zone operation, and the likelihood of meeting rotating reserve capacity across various scheduling scenarios. Both the deterministic optimal scheduling scheme and the stochastic optimal scheduling scheme fully meet the rotating reserve and vibration zone limitations, with lower overall water consumption compared with the simulated scheduling scheme (1.7% and 1.2%, respectively). However, the historical scheduling (simulation) scenario falls short of satisfying these conditions completely. Adhering strictly to the vibration zone limits and rotating standby limits in the historical dispatch (simulation) scenario could potentially lead to further flow increases.

Table 4. Comparison of economic operation results for a typical day under different scheduling scenarios.

Evaluation Metrics	Historical Scheduling (Simulation)	Deterministic Optimization Scheduling	Stochastic Optimization Scheduling
Total water consumption (100,000 m^3)	49.49	48.65	48.86
Probability of non-vibration zone operation (%)	91.2	100	100
Load standby fulfillment probability (%)	83.6	100	100

If the proposed model and algorithm are implemented, the hydropower station could conserve 63,000 m^3 of water in a single day. Additionally, based on the operating efficiency of the supplemental system in the area (3 m^3 = 1 kWh), power generation would increase by 21,000 kWh in a day and by 7.665 × 106 kWh annually. The station's annual power generation benefit would also rise by 1,533,000 Yuan, resulting in a substantial economic advantage. This economic benefit is noteworthy at 1.533 million yuan, especially considering the context of a microgrid with small hydropower and a tiny photovoltaic power station. If the non-steady state strategy is applied to a large terraced multi-energy complementary system, the economic benefits become even more remarkable. Calculations reveal that the electricity consumption of 6,017,025 kWh would result in carbon emissions of 6,017,025 kg. The combustion of 1 ton of standard coal energy produces approximately 2.6 tons of carbon dioxide. Therefore, by emphasizing energy conservation and emission reduction, there is potential to reduce carbon dioxide emissions by 15,644.265 tons annually. This approach aligns with the principle of sustainable development, aiming to balance economic growth with the preservation of critical environmental resources such as the atmosphere, fresh water, oceans, land, and forests. Adopting sustainable practices presents needs without compromising the ability of future generations to meet their own needs, ensuring harmonious and peaceful coexistence while experiencing the positive impacts of sustainable development.

5. Conclusions

This study introduces an innovative two-layer nested model, integrating the improved PSO algorithm and the trial run of the SOA. The outer layer utilizes the improved PSO algorithm to optimize the output distribution of each power plant in the HPV system, with the goal of minimizing the residual load. The inner layer employs the SOA for trial operation, optimizing the start/stop sequence of the hydropower station units to minimize flow consumption under the load conditions obtained after the outer layer optimization. The model is applied to optimize the multi-constraint and high-dimensional HPV complementary system in the complex terrain of the southwest plateau area of China. It optimizes both the deterministic scenario and stochastic optimization scenario of the HPV complementary system, obtaining 20 statistical results of the optimal outcomes, surpassing historical data simulation. Furthermore, the optimization results are achieved within 5 min each time. This study compared a historical scenario scheduling simulation scheme, a deterministic optimal scheduling scheme considering perfect photovoltaic and runoff predictions, and a stochastic optimal scheduling scheme considering uncertainty in photovoltaic and runoff forecasts. The following conclusions can be drawn from the findings of this study:

(1) In a complementary system, the uncertainty in photovoltaic output and inflow runoff can complement each other by optimizing and adapting in a double-layer nested model.
(2) The water head range, output range, and vibration range of the hydropower station influence the adjustable range of the unit. A small change in water consumption can bring about a significant change in the adjustable range. The proposed two-dimensional coding strategy effectively handles the continuous start/stop constraints of the unit, significantly reducing the number of optimization variables and achieving dimensionality reduction.
(3) The proposed double-layer nested optimization algorithm effectively generates an economic operation plan within a short time. By trial-computing the inner-layer optimization results, a daily dispatch plan with 384 optimized variables can be obtained in just 5 min.
(4) Compared with historical dispatch simulation scenarios, the deterministic optimization and stochastic optimization scenarios reduced water consumption by 1.7% and 1.2% respectively. This not only confirms the superiority of the model but also demonstrates the advantages of coupling photovoltaic and runoff prediction for short-term water dispatching, resulting in a complementary gain effect for water and light.

The double-layer nested model, combining the improved PSO algorithm with the trial operation of the SOA, effectively and consistently addresses the collaborative optimization challenge in multi-energy complementary systems within complex plateau scenarios. This model is readily applicable to diverse regions, with the exclusion of extreme areas like volcanoes and polar regions. Specifically designed for the southwest plateau region of China, endowed with abundant natural resources but marked by intricate terrain and harsh climate conditions, the design model accommodates various constraints, rendering it widely applicable. If extended to different renewable energy systems, only the objective function and constraints of the outer improved PSO algorithm require modification. This facilitates the optimization of output capacity allocation for photovoltaic power stations and hydropower stations, integrating them into the combined output of wind, solar, and other emerging energy power stations. The model can adeptly respond to the higher-frequency control demands inherent in the new paradigm of wind, solar, and energy storage. As the number of iterations increases, the model converges toward the optimal solution with enhanced timeliness and accuracy. Objectively, this model safeguards and reinforces the production and regenerative capacities of environmental systems, maximizes the positive impact of economic growth, preserves the quality of natural resources, and enhances human well-being without surpassing the ecosystem's support capacity.

Author Contributions: Conceptualization, Z.L. and Z.H.; methodology, Z.L., Z.H. and N.L.; software, Z.H.; validation, Z.H. and N.L.; writing—original draft preparation, Z.H.; writing—review and editing, Z.L. and X.Z.; visualization, N.L., L.D. and H.C.; supervision, Z.L. (Z.H. is the first author and Z.L. is the corresponding author). All authors have read and agreed to the published version of the manuscript.

Funding: This research received no external funding.

Institutional Review Board Statement: Not applicable.

Informed Consent Statement: Not applicable.

Data Availability Statement: The data presented in this study are available on request from the corresponding author.

Conflicts of Interest: The authors declare no conflict of interest.

Glossary

IPSO-SOAT	Improved Particle Swarm Optimization Algorithm with Weight Coefficients-Stepwise Optimization Algorithm Trial Operational Model
PV	Photovoltaic
HES	Hybrid Energy System
UC	Unit Combination
RO	Robust Optimization
BNOA	Bilayer Nested Optimization Approach
p_n	Photovoltaic prediction, Uncertain Characterization of PV Output Force (MW)
p_f	Typical daily values after clustering of photovoltaic historical data (MW)
e	Optical prediction error values, following a normal distribution (MW)
F	Objective function for economic dispatch operations (m)
$\mu_{n,t}$	On/off status of the unit, n is a 0–1 variable (1 for unit on, 0 for unit off)
$r_{m,n,t}$	Consumption rate of the nth PV unit at time slot t for the mth PV scenario (m)
Δt	Stepsize (scheduling time slot length) (min)
$P^h_{m,nt}$	Hydroelectric unit transient output at time period t of the mth scenario (MW)
$h_{m,t}$	Head at time period t of the mth scene (m)
$h^{loss}_{m,t}$	head loss (m)
$z^{up}_{m,t}$	Water level before runoff to hydroelectric plants (m)
$z^{down}_{m,t}$	Water level after runoff from hydroelectric plants (m)
$v_{m,t}$	Storage capacity at the beginning of time period t (m^3)
$v_{m,t+1}$	Storage capacity at the end of time period t (m^3)

I_t	Average incoming flow in time period t
Q_t^{min}	Upper limit of the flow rate into the reservoir of the hydropower plant in time period t (m^3/s)
Q_t^{max}	Lower limit of the flow rate into the reservoir of the hydropower plant in time period t (m^3/s)
Q_t	Incoming flow at hydroelectric power station at time period t (m^3/s)
v^-	Lower limit of hydroelectric power plant capacity (m^3)
v^+	Upper limit of hydroelectric power plant capacity (m^3)
LP_t	spinning reserve margin (MW)
ΔP	Upper speed limit for unit raising/lowering (MW)
k	Time code
SU_N	Minimum on-line time of the unit
$\mathrm{SD_N}$	Maximum online time of the unit
$\mathrm{su_{n,k}}$	Unit power-on action (1 for power on, 0 for power off)
$\mathrm{sd_{n,k}}$	Unit shutdown action (1 for shutdown, 0 for power on)
P_n^{low}	Lower limit of unit vibration zone (MW)
P_n^{up}	Upper limit of unit vibration zone (MW)
v_i^d	The velocity of the ith particle in the d-dimension (m/s)
x_i^d	Position of the ith particle in d-dimension (one solution of the objective function)
w	Inertia weighting factor
r_1	Self-learning factor
r_2	Group Learning Factor
HP_t^n	Hydroelectric power output at time t in the nth sample scenario (MW)
ΔhP_t^n	Hydroelectric output fluctuations at time t in the nth sample scenario (MW)
H_{pe}	Hydroelectric Power Plant Expected Output Scenario Set (MW)
HP_t^{up}	Upper boundary value of hydroelectric power plant output in Stepsize t (MW)
HP_t^{low}	Lower boundary value of hydropower plant output in Stepsize t (MW)
NT	The algorithm optimizes the total number of variables
ou_T	Number of units on-line in each dispatch period during the entire dispatch period T
so	Total number of consecutive periods during the scheduling period in which the number of units in operation remains unchanged
tn_{so}	Indicates the time node at which the state of the unit is about to change
$\mathrm{su_{so}}$	Indicates the number of online units for each stabilization period.
$R_{d,t}^*$	total output
$f_{rph}(p_{d,t},h_t)$	Generation water consumption flow rate of unit j when net load is $\mathrm{p_{d,t}}$ and net head is $\mathrm{h_t}$

References

1. Zhou, X.; Chen, S.; Lu, Z.; Huang, Y.; Ma, S.; Zhao, Q. Technology Features of the New Generation Power System in China. *Proc. CSEE* **2018**, *38*, 1893–1904.
2. Kober, T.; Schiffer, H.W.; Densing, M.; Panos, E. Global energy perspectives to 2060—WEC's World Energy Scenarios 2019. *Energy Strategy Rev.* **2020**, *31*, 100523. [CrossRef]
3. Wang, D.D.; Sueyoshi, T. Climate change mitigation targets set by global firms: Overview and implications for renewable energy. *Renew. Sustain. Energy Rev.* **2018**, *94*, 386–398. [CrossRef]
4. Tafuni, A.; Giannotta, A.; Mersch, M.; Pantaleo, A.M.; Amirante, R.; Markides, C.N.; De Palma, P. Thermo-economic analysis of a low-cost greenhouse thermal solar plant with seasonal energy storage. *Energy Convers. Manag.* **2023**, *288*, 117123. [CrossRef]
5. Ma, X.; Zhai, Y.; Zhang, T.; Yao, X.; Hong, J. What changes can solar and wind power bring to the electrification of China compared with coal electricity: From a cost-oriented life cycle impact perspective. *Energy Convers. Manag.* **2023**, *289*, 117162. [CrossRef]
6. Guo, Y.; Ming, B.; Huang, Q.; Wang, Y.; Zheng, X.; Zhang, W. Risk-averse day-ahead generation scheduling of hydro–wind–photovoltaic complementary systems considering the steady requirement of power delivery. *Appl. Energy* **2022**, *309*, 118467. [CrossRef]
7. Tian, C.C. Function Remolding of Hydropower Systems for Carbon Neutral and Its Key Problems. *Autom. Electr. Power Syst.* **2021**, *45*, 29–36.
8. Nematollahi, O.; Hoghooghi, H.; Rasti, M.; Sedaghat, A. Energy demands and renewable energy resources in the Middle East. *Renew. Sustain. Energy Rev.* **2016**, *54*, 1172–1181. [CrossRef]
9. Luo, S.; Hu, W.; Huang, Q.; Han, X.; Chen, Z. Optimization of Photovoltaic/Small Hydropower/Pumped Storage Power Station System Sizing under the Market Mechanism. *Trans. China Electrotech. Soc.* **2020**, *35*, 2792.

10. Braff, W.A.; Mueller, J.M.; Trancik, J.E. Value of storage technologies for wind and solar energy. *Nat. Clim. Chang.* **2016**, *6*, 964–969. [CrossRef]
11. Guo, S.; Liu, Q.; Sun, J.; Jin, H. A review on the utilization of hybrid renewable energy. *Renew. Sustain. Energy Rev.* **2018**, *91*, 1121–1147. [CrossRef]
12. Yanmei, Z.; Shijun, C.; Guangwen, M.; Xiaoyan, H.; Liang, W. Short-Term Complementary Operation of Hydro-Photovoltaic Integrated System Considering Power Generation and Output Fluctuation. *Trans. China Electrotech. Soc.* **2020**, *35*, 2769–2779.
13. Ashok, S. Optimised model for community-based hybrid energy system. *Renew. Energy* **2007**, *32*, 1155–1164. [CrossRef]
14. Zou, S.; Zhang, N.; Wei, B. A capacity optimization and scheduling scheme of a multi-energy complementary power station considering energy trading. *Front. Energy Res.* **2023**, *11*, 1194139. [CrossRef]
15. Wang, S.; Jia, R.; Shi, X.; An, Y.; Huang, Q.; Guo, P.; Luo, C. Hybrid Time-Scale Optimal Scheduling Considering Multi-Energy Complementary Characteristic. *IEEE Access* **2021**, *9*, 94087–94098. [CrossRef]
16. Li, J.; Luo, G.; Li, T.; Gao, L.; Liang, X.; Hu, J.; Cao, Y.; Qi, L.; Liu, X.; Huo, M. Impact on traditional hydropower under a multi-energy complementary operation scheme: An illustrative case of a 'wind–photovoltaic–cascaded hydropower plants' system. *Energy Strategy Rev.* **2023**, *49*, 101181. [CrossRef]
17. Li, H.; Liu, P.; Guo, S.; Ming, B.; Cheng, L.; Yang, Z. Long-term complementary operation of a large-scale hydro-photovoltaic hybrid power plant using explicit stochastic optimization. *Appl. Energy* **2019**, *238*, 863–875. [CrossRef]
18. Yang, Y.; Zhou, J.; Liu, G.; Mo, L.; Wang, Y.; Jia, B.; He, F. Multi-plan formulation of hydropower generation considering uncertainty of wind power. *Appl. Energy* **2020**, *260*, 114239. [CrossRef]
19. Zhu, F.; Zhong, P.; Xu, B.; Liu, W.; Wang, W.; Sun, Y.; Chen, J.; Li, J. Short-term stochastic optimization of a hydro-wind-photovoltaic hybrid system under multiple uncertainties. *Energy Convers. Manag.* **2020**, *214*, 112902. [CrossRef]
20. Shayan, M.E.; Najafi, G.; Ghobadian, B.; Gorjian, S.; Mazlan, M. A novel approach of synchronization of the sustainable grid with an intelligent local hybrid renewable energy control. *Int. J. Energy Environ. Eng.* **2023**, *14*, 35–46. [CrossRef]
21. Shayan, M.E.; Najafi, G.; Ghobadian, B.; Gorjian, S.; Mamat, R.; Ghazali, M.F. Multi-microgrid optimization and energy management under boost voltage converter with Markov prediction chain and dynamic decision algorithm. *Renew. Energy* **2022**, *201*, 179–189. [CrossRef]
22. Shou-ren, Z. Development and utilization of hydropower resources in China: Opportunity and challenges. *J. Hydraul. Eng.* **2007**, *1*, 9350.
23. Yi, J.; Labadie, J.W.; Stitt, S. Dynamic Optimal Unit Commitment and Loading in Hydropower Systems. *J. Water Res. Plan. Man.* **2003**, *129*, 388–398. [CrossRef]
24. Anoune, K.; Bouya, M.; Astito, A.; Abdellah, A.B. Sizing methods and optimization techniques for PV-wind based hybrid renewable energy system: A review. *Renew. Sustain. Energy Rev.* **2018**, *93*, 652–673. [CrossRef]
25. Chen, L.; Ge, L.; Wang, D.; Zhong, W.; Zhan, T.; Deng, A. Multi-objective water-sediment optimal operation of cascade reservoirs in the Yellow River Basin. *J. Hydrol.* **2022**, *609*, 127744. [CrossRef]
26. Yuan, X.; Yu, H.; Liang, J.; Xu, B. A novel density peaks clustering algorithm based on K nearest neighbors with adaptive merging strategy. *Int. J. Mach. Learn. Cybern.* **2021**, *12*, 2825–2841. [CrossRef]
27. Salomon, S.; Avigad, G.; Fleming, P.J.; Purshouse, R.C. Active Robust Optimization: Enhancing Robustness to Uncertain Environments. *IEEE Trans. Cybern.* **2014**, *44*, 2221–2231. [CrossRef] [PubMed]
28. Jensen, M.T. Generating robust and flexible job shop schedules using genetic algorithms. *IEEE Trans. Evolut. Comput.* **2003**, *7*, 275–288. [CrossRef]
29. Wiesmann, D.; Hammel, U.; Back, T. Robust design of multilayer optical coatings by means of evolutionary algorithms. *IEEE Trans. Evolut. Comput.* **1998**, *2*, 162–167. [CrossRef]
30. Qiu, H.; Gu, W.; Xu, X.; Pan, G.; Liu, P.; Wu, Z.; Wang, L. A Historical-Correlation-Driven Robust Optimization Approach for Microgrid Dispatch. *IEEE Trans. Smart Grid* **2021**, *12*, 1135–1148. [CrossRef]
31. Mahdi, M.; Xueqian, S.; Gai, Q.; Basirialmahjough, M.; Yuan, H. Improving robustness of water supply system using a multi-objective robust optimization framework. *Environ. Res.* **2023**, *232*, 116270. [CrossRef] [PubMed]
32. Guo, Q.; Guo, T.; Tian, Q.; Nojavan, S. Optimal robust scheduling of energy-water nexus system using robust optimization technique. *Comput. Chem. Eng.* **2021**, *155*, 107542. [CrossRef]
33. Nag, K.; Pal, T.; Mudi, R.K.; Pal, N.R. Robust Multiobjective Optimization with Robust Consensus. *IEEE Trans. Fuzzy Syst.* **2018**, *26*, 3743–3754. [CrossRef]
34. San, L.C.; Fulong, L. Press Conference of the National Energy Administration on the Energy Situation in the First Half of the Year. In Proceedings of the China National Energy Administration Routine Press Conference, Beijing, China, 1 July 2022.
35. Yousri, D.; Farag, H.E.Z.; Zeineldin, H.; El-Saadany, E.F. Integrated model for optimal energy management and demand response of microgrids considering hybrid hydrogen-battery storage systems. *Energy Convers. Manag.* **2023**, *280*, 116809. [CrossRef]
36. Prasanna, A.; Dorer, V.; Vetterli, N. Optimisation of a district energy system with a low temperature network. *Energy* **2017**, *137*, 632–648. [CrossRef]
37. Brentan, B.M.; Carpitella, S.; Izquierdo, J.; Luvizotto, E.; Meirelles, G. District metered area design through multicriteria and multiobjective optimization. *Math. Method Appl. Sci.* **2022**, *45*, 3254–3271. [CrossRef]
38. Liu, Y.; Wang, G.; Zhou, J.; Dai, R.; Yu, F. Optimal planning strategy for energy internet zones based on interval optimization. *Energy Rep.* **2020**, *6*, 1255–1261. [CrossRef]

39. Zhang, Y.; Lian, J.; Ma, C.; Yang, Y.; Pang, X.; Wang, L. Optimal sizing of the grid-connected hybrid system integrating hydropower, photovoltaic, and wind considering cascade reservoir connection and photovoltaic-wind complementarity. *J. Clean. Prod.* **2020**, *274*, 123100. [CrossRef]
40. Ming, B.; Liu, P.; Guo, S.; Zhang, X.; Feng, M.; Wang, X. Optimizing utility-scale photovoltaic power generation for integration into a hydropower reservoir by incorporating long- and short-term operational decisions. *Appl. Energy* **2017**, *204*, 432–445. [CrossRef]